Research Article

Study on the Vector Quadrilateral Isoparametric Shell Element with Shear Deformation

Zhen Wang [1,2,3] **Yang Zhao,** [1,4] **Zhi Ding,** [1,2,3] **and Huiping Tang** [1,2]

[1] *Department of Civil Engineering, Zhejiang University City College, Hangzhou 310015, China*
[2] *Advanced Materials Additive Manufacturing Innovation Research Center, Zhejiang University City College, Hangzhou 310015, China*
[3] *Key Laboratory of Safe Construction and Intelligent Maintenance for Urban Shield Tunnels of Zhejiang Province, Hangzhou 310015, China*
[4] *College of Civil Engineering and Architecture, Zhejiang University, Hangzhou 310058, China*

Correspondence should be addressed to Zhen Wang; wangzhen@zucc.edu.cn

Based on the linear superposition of the quadrilateral isoparametric membrane element and quadrilateral Mindlin plate element, basic vector formulas for the quadrilateral isoparametric shell element with the shear deformation is derived. Two different coordinate modes for updating the particle displacement and the element node internal force are put forward. The uniform numerical solution for an irregular quadrilateral element is realized by the isoparametric integral scheme along the element plane. Then, the bilinear elastoplastic constitutive of material is introduced into the vector finite shell element, and the nonlinear effect of the material is realized based on the integral method along the thickness. On this basis, the nonlinear calculation and analysis program of the quadrilateral isoparametric shell element is developed. Numerical example results show that the static and dynamic analysis, large deformation and large rotation analysis, and buckling analysis can all be well performed for the shell structures by the developed program, which verifies the validity of theoretical derivation and computer program.

1. Introduction

The shell structure is a two-dimensional element structure, which is widely used in engineering structures, including hyperbolic flat shells, spherical shells, cylindrical shells, and surface structures with complex surface structures and boundaries [1–5]. Under the action of external loading, the shell structure has both in-plane tensile deformation and out-of-plane bending deformation, which can be regarded as the linear superposition of membrane elements and plate elements.

The shell elements include planar shell elements and surface shell elements, and the former is relatively simple and has good precision. Green et al. [6] first adopted a triangular flat shell element and applied it to a shell structure of arbitrary shape. Zienkiewicz [7] proposed the analysis theory that combined membrane element and plate element to simulate planar shell element. Bathe and Ho [8] developed the basic theory for isoparametric thin shell element obtained from the surface of higher-order shape function, which was analyzed and compared with the calculation accuracy of thin shell element composed by linear superposition film element and the plate element. It was shown that the latter method had good accuracy and its theoretical formula was simple and easy to apply. Yang et al. [9] pointed out that by assuming the value of normal rotation stiffness to avoid stiffness matrix singularity, the obtained convergence result might be poor. It is suggested that the rotation degree of freedom should be considered separately as one of the degrees of freedom for the shell element to obtain more effective and accurate calculation results. In terms of the shear deformation of shell elements, there are some relevant literature studies. Wang et al. [10] proposed a simple first-order shear deformation shell theory (S-FSDST) for free and transient vibration analysis of composite laminated open cylindrical shells with general boundary conditions.

Lezgy–Nazargah and Salahshuran [11] presented a novel mixed-field theory with a relatively low number of unknown variables for bending and vibration analysis of multilayered composite plates. Lezgy–Nazargah [12] developed a high-performance finite element model for bending and vibration analysis of thick plates based on the parametrized mixed variational principle. Lezgy–Nazargah and Meshkani [13] proposed a four-node quadrilateral partial mixed plate element with low degrees of freedom (dofs) for static and free vibration analysis of functionally graded material (FGM) plates rested on Winkler–Pasternak elastic foundations.

Vector Form Intrinsic Finite Element (VFIFE) is a new dynamic calculation analysis method based on particle mechanics and vector operation mode [14–16]. This method is based on the second law of motion of a particle and belongs to a class of discrete element method. It does not involve mathematical continuous function and has a simple theory and no iteration. By means of vector operation mode, the relations among variables such as force (moment), displacement, and acceleration are expressed by particles, while the numerical calculation results of multi-particle discretization approach the approximate value of the real unique solution, and each particle is calculated separately and cyclically step by step. Therefore, the VFIFE method is more convenient for analyzing the dynamic behavior of complex structures such as large deformation, large rotation, stability, collision, and fracture. At present, some research achievements have been made on two-dimensional plate and shell element of vector finite element. Wu et al. [17] studied the vector formula theory of triangular membrane element and applied it to large deformation and large rotation analysis of membrane structure. Wang et al. [18] studied the vector formula theory of triangular thin shell element and the treatment and application of elastic-plastic materials constitutive model. However, the existing literature of VFIFE mainly focuses on the research of triangular element, and there is no relevant study on the theory and application of quadrilateral isoparametric shell element, and the influence of shear deformation on thick shell is not involved.

In this paper, by linear superposition of quadrilateral isoparametric membrane element and quadrilateral Mindlin plate element, the basic vector formula of quadrilateral isoparametric shell element with shear deformation is derived firstly. Two different coordinate modes for solving particle displacement and internal force of element node and the integration of internal force for element node along element thickness and plane are then proposed. The bilinear elastoplastic material constitutive model is used to deal with the nonlinear effect of structure in vector calculation. On this basis, the nonlinear calculation and analysis program of quadrilateral isoparametric shell element is developed, and the validity of derived formulas and program codes is verified by analysis of typical examples.

2. Theory of Vector Quadrilateral Isoparametric Shell

The VFIFE method discretizes structure into two parts including mass particles and massless elements. And, the

solving process includes three steps: the total displacement of particles, the pure deformation displacement of nodes, and the internal force of nodes. The shell element is superimposed of the quadrilateral membrane element and Mindlin plate element with shear deformation in this paper.

In this section, equation (1) is obtained by using the relevant formula in literature [19]. Equations (2)–(9) are the formulas of quadrilateral isoparametric shell element under the VFIFE theoretical framework derived in this paper, without reference to other literatures. Equations (10)–(32) are the relevant formulas of quadrilateral isoparametric shell element under the VFIFE theoretical framework derived with reference to the literature [19, 20], which belong to the original content, and have been cited in Sections 2.2 and 2.3, respectively.

2.1. Total Displacement of Particles.
The particle motion equation is obtained through Newton's second law, which is given by the following equation:

$$\begin{cases} \mathbf{M}\ddot{\mathbf{x}} + \alpha\mathbf{M}\dot{\mathbf{x}} = \mathbf{F}, \\ \mathbf{I}\ddot{\boldsymbol{\theta}} + \alpha\mathbf{I}\dot{\boldsymbol{\theta}} = \mathbf{F}_{\boldsymbol{\theta}}, \end{cases} \tag{1}$$

where $\mathbf{M}$ and $\mathbf{I}$ are the mass matrix and moment of inertia matrix, respectively, $\mathbf{x}$ is the linear coordinate vector, θ is the angular coordinate vector, $\mathbf{F} = \mathbf{f}^{\text{ext}} + \mathbf{f}^{\text{int}}$ is the resultant force vector, $\mathbf{F}_{\theta} = \mathbf{f}_{\theta}^{\text{ext}} + \mathbf{f}_{\theta}^{\text{int}}$ is the resultant moment vector, and the superscript "ext" and "int", respectively, represent the external force and internal force, α is the damping parameters.

During each update substep, the central difference formula is used for numerical calculation, and the total particle displacement is gradually obtained through a loop substep update. For the quadrilateral isoparametric shell element in this paper, $\mathbf{f}^{\text{int}}$ and $\mathbf{f}_{\theta}^{\text{int}}$ in equation (1) are obtained from coordinate definition mode I, $\mathbf{x}$ and θ in equation (1) are obtained from coordinate definition mode II, which are described in Section 3.1.

2.2. Pure Deformation Displacement of Element Nodes.
By introducing the inverse motion concept, the rigid displacement is deducted from the total displacement of a particle to get pure deformation displacement for element nodes. The actual spatial quadrilateral of the element is transformed into a planar quadrilateral by the projection method, which is that of coordinate definition mode I. The actual coordinate vectors of the four element nodes i ($i = a, b, c, d$) are denoted in this section as $\mathbf{x}_i$, and the unit edge vector of the spatial quadrilateral $\mathbf{e}_{kl}$ is given by the following equation:

$$e_{kl} = \frac{x_l - x_k}{|x_l - x_k|} \ (kl = ab, bc, cd, da), \tag{2}$$

where k and l are two adjacent points of the spatial quadrilateral.

The unit normal vector of the plane corresponding to two adjacent edges of the spatial quadrilateral $\mathbf{n}_j^0$ is given by the following equation:

$$\mathbf{n}_j^0 = \frac{e_{kl} \times e_{mn}}{|e_{kl} \times e_{mn}|} \ (kl, mn = ab, bc, cd, da; j = 1, 2, 3, 4), \quad (3)$$

where kl and mn are two adjacent edges of the spatial quadrilateral.

The unit mean normal vector of the projection plane $\mathbf{n}^0$ is given by the following equation:

$$\mathbf{n}^0 = \frac{n}{|n|} = \left(\frac{1}{4}\sum_{j=1}^{4} n_j^0\right) \Big/ \left|\frac{1}{4}\sum_{j=1}^{4} n_j^0\right| (j = 1, 2, 3, 4), \quad (4)$$

where $n = 1/4\sum_{j=1}^{4} n_j^0$ is the mean normal vector of the projection plane.

The projection coordinate vectors on the projection plane of element node i ($i = a, b, c, d$) are denoted as $\overline{\mathbf{x}}_i$, which is given by the following equation:

$$\overline{x}_i = x_c + \left[dx_i - (dx_i \cdot \mathbf{n}^0)\mathbf{n}^0\right], \quad (5)$$

where $\mathbf{x}_C$ is the coordinate vector of the centroid point C, $dx_i = x_i - x_C$ is the distance vector for element nodes i relative to centroid point C.

The projection distance vectors of projection points of element nodes i relative to centroid point C are denoted as $d\overline{\mathbf{x}}_i$, which is given by the following equation:

$$d\overline{\mathbf{x}}_i = \overline{\mathbf{x}}_i - x_c, \quad (6)$$

where $\overline{\mathbf{x}}_i$ is the coordinate vector of the projection point of the element node i.

The actual angular coordinate vectors of the four element nodes i ($i = a, b, c, d$) are denoted as θ_i, then the rotational angle of the element node caused by projection $d\theta_i$ (that is, the rotation angle from dx_i to $d\overline{x}_i$ with unit vector $\mathbf{n}_{pi}^0$ as the rotation axis) is given by the following equation:

$$d\theta_i = \cos^{-1}\left(\frac{dx_i \cdot d\overline{x}_i}{|dx_i||d\overline{x}_i|}\right), d\theta_i \in [0, \pi], \quad (7)$$

where $\mathbf{n}_{pi}^0 = (d\mathbf{x}_i \times d\overline{\mathbf{x}}_i)/|d\mathbf{x}_i \times d\overline{\mathbf{x}}_i|$.

The rotational angular displacement vector of element node $d\theta_i$ is given by the following equation:

$$d\boldsymbol{\theta}_i = d\boldsymbol{\theta}_i n_{pi}^0. \quad (8)$$

The projection angular coordinate vector of element node $\overline{\theta}_i$ is given by the following equation:

$$\overline{\boldsymbol{\theta}}_i = \theta_i + d\theta_i. \quad (9)$$

After projection method processing, the spatial quadrilateral element is transformed into the planar quadrilateral element, corresponding to the coordinate definition mode I ($\overline{\mathbf{x}}_i, \overline{\mathbf{x}}_i', \overline{\theta}_i, \overline{\theta}_i', \mathbf{n}, \mathbf{n}'$), where $\overline{\mathbf{x}}_i$ and $\overline{\mathbf{x}}_i'$ are the coordinate vectors for projection points of element nodes i corresponding to the beginning and end of particle motion time substep, $\overline{\theta}_i$ and $\overline{\theta}_i'$ are the angular coordinate vectors for projection points of element nodes i corresponding to the beginning and end of particle motion time substep, $\mathbf{n}$ and $\mathbf{n}'$ are the mean normal vectors of the projection planes corresponding to the beginning and end of particle motion time substep. The total linear displacement vectors and total angular displacement vectors of element nodes i are, respectively, $\mathbf{u}_i = \overline{\mathbf{x}}_i' - \overline{\mathbf{x}}_i$ and $\mathbf{u}_{\theta i} = \overline{\theta}_i' - \overline{\theta}_i$.

The spatial motion for the projection plane (i.e., planar quadrilateral) includes rigid body translation, out-of-plane rigid body rotation, in-plane rigid body rotation, and pure deformation displacement. The specific derivation is similar to the triangle plate element theory in reference [19], and only the main derivation formulas are given in this paper.

Rigid body translation is taken as the total linear displacements vector $\mathbf{u}_a$ for reference node a, then the relative linear displacements $\Delta\eta_i$ and relative angular displacements $\Delta\eta_{\theta i}$ for element node i after deducting the rigid body translation are given by the following equation:

$$\begin{cases} \Delta\boldsymbol{\eta}_a = 0, \Delta\boldsymbol{\eta}_i = u_i - u_a, & (i = b, c, d), \\ \Delta\boldsymbol{\eta}_{\theta i} = u_{\theta i}, & (i = a, b, c, d), \end{cases} \quad (10)$$

Rigid body rotation is estimated based on the projection plane, including out-of-plane rigid body rotation and in-plane rigid body rotation. The opposite direction of rotation is inverse rotation and the linear displacement $\Delta\eta_{i-op}^r$ and angular displacement $\Delta\eta_{\theta i-op}^r$ of the out-of-plane reverse rigid body rotation are given by the following equation:

$$\theta_1 \begin{cases} \Delta\boldsymbol{\eta}_{a-op}^r = 0, \Delta\boldsymbol{\eta}_{i-op}^r = \left(R_{op}^T(-\theta_1) - I\right)r_{ai}'' = R_{op}^*(-\theta_1) \cdot r_{ai}'', & (i = b, c, d), \\ \Delta\boldsymbol{\eta}_{\theta i-op}^r = -\theta_1 = -\theta_1 n_{op}^0, & (i = a, b, c, d), \end{cases} \quad (11)$$

where θ_1 is the out-of-plane rotational angle of projection plane (that is, the rotational angle from $\mathbf{n}$ to $\mathbf{n}''$ with unit vector $\mathbf{n}_{op}^0 = (\mathbf{n} \times \mathbf{n}'')/|\mathbf{n} \times \mathbf{n}''| = \left\{l_{op} \ m_{op} \ n_{op}\right\}^T$ as the rotational axis) which is given by equation (12), $-\theta_1$ is the out-of-plane inverse rotational angle of the projection plane, θ_1 is the out-of-plane rotational angle vector of the projection plane, $\mathbf{R}_{op}^*(-\theta_1)$ is the out-of-plane inverse

rotation matrix which is given by equation (13), $\mathbf{r}_{ai}'' = \overline{\mathbf{x}}_i'' - \overline{\mathbf{x}}_a'' = \overline{\mathbf{x}}_i' - \overline{\mathbf{x}}_a'$ is the edge vector of the projection planar element (i.e., planar element consisting of projection points of element nodes) after deducting the rigid body translation, $\mathbf{x}_i''$ is the coordinate vector of the projection point of element node i after deducting the rigid body translation.

$$\mathbf{n}'' \theta_1 = \cos^{-1}\left(\frac{n \cdot n''}{|n||n''|}\right), \theta_1 \in [0, \pi], \qquad (12)$$

where $\mathbf{n}''$ are the mean normal vectors of the projection planes after deducting the rigid body translation which can be obtained by substituting $\overline{\mathbf{x}}_i''$ for $\mathbf{x}_i$ in equation (2)~ equation (4).

$$\mathbf{R}_{op}^*(-\theta_1) = [1 - \cos(-\theta_1)]A_{op}^2 + \sin(-\theta_1)A_{op}, \qquad (13)$$

where $\mathbf{A}_{op} = \begin{bmatrix} 0 & -n_{op} & m_{op} \\ n_{op} & 0 & -l_{op} \\ -m_{op} & l_{op} & 0 \end{bmatrix}$.

The linear displacements $\Delta\eta_{i-ip}^{r}$ and angular displacements $\Delta\eta_{\theta i-ip}^{r}$ for the in-plane reverse rigid body rotation are given by the following equation:

$$\begin{cases} \Delta\boldsymbol{\eta}_{a-ip}^{r} = 0, \Delta\boldsymbol{\eta}_{i-ip}^{r} = \left(R_{ip}^{T}(-\theta_2) - I\right)r_{ai}'' = R_{ip}^*(-\theta_2) \cdot r_{ai}'', & (i = b, c, d), \\ \Delta\boldsymbol{\eta}_{\theta i-ip}^{r} = -\theta_2 = -\theta_2 n_{ip}^0, & (i = a, b, c, d), \end{cases} \qquad (14)$$

where θ_2 is the in-plane rotational angle of projection plane (that is, the average in-plane rotational angle of the projection plane with the unit vector $\mathbf{n}_{ip}^0 = \mathbf{n}^0 = \mathbf{n}/|\mathbf{n}| = \{l_{ip} \quad m_{ip} \quad n_{ip}\}^T$ as the rotation axis) which is given by equation (15), $-\theta_2$ is the in-plane inverse rotational angle of the projection plane, θ_2 is the in-plane rotational angle vector of the projection plane, $\mathbf{R}_{ip}^*(-\theta_2)$ is the in-plane inverse rotation matrix which is given by equation (18), $\mathbf{r}_{ai}''' = \overline{\mathbf{x}}_i''' - \overline{\mathbf{x}}_a''' = \overline{\mathbf{x}}_i' - \overline{\mathbf{x}}_a' + \Delta\eta_{i-op}^r$ is the edge vector of the projection planar element (i.e., planar element consisting of projection points of element nodes) after deducting the rigid body translation and the out-of-plane rigid body rotation, $\mathbf{x}_i'''$ is the coordinate vector of the projection point of element node i after deducting the rigid body translation and the out-of-plane rigid body rotation.

$$\theta_2 = \frac{(\Delta\varphi_a + \Delta\varphi_b + \Delta\varphi_c + \Delta\varphi_d)}{4}, \theta_2 \in [-\pi, \pi], \qquad (15)$$

where $\Delta\varphi_i$ $(i = a, b, c, d)$ is the in-plane rotational angle of element i which is given by the following equations:

$$|\Delta\varphi_i| = \cos^{-1}\left(e_i \cdot \mathbf{e}_i'''\right), (i = a, b, c, d), \qquad (16)$$

where $\mathbf{e}_i = (\overline{\mathbf{x}}_i - \overline{\mathbf{x}}_C)/|\overline{\mathbf{x}}_i - \overline{\mathbf{x}}_C|$, $\mathbf{e}_i''' = (\overline{\mathbf{x}}_i''' - \overline{\mathbf{x}}_C)/|\overline{\mathbf{x}}_i''' - \overline{\mathbf{x}}_C|$, $\overline{\mathbf{x}}_C$ is the coordinate vector of the projection point of centroid point C.

$$\begin{cases} \Delta\varphi_i = |\Delta\varphi_i|, & \text{when } e_i \times e_i''' \text{ and } n^0 \text{ are in same direction}, \\ \Delta\varphi_i = |\Delta\varphi_i|, & \text{when } e_i \times e_i''' \text{ and } n^0 \text{ are in opposite direction}, \end{cases} \qquad (17)$$

$$\mathbf{R}_{ip}^*(-\theta_2) = [1 - \cos(-\theta_2)]A_{ip}^2 + \sin(-\theta_2)A_{ip}, \qquad (18)$$

where $\mathbf{A}_{ip} = \begin{bmatrix} 0 & -n_{ip} & m_{ip} \\ n_{ip} & 0 & -l_{ip} \\ -m_{ip} & l_{ip} & 0 \end{bmatrix}$.

After deducting the rigid body translation, the out-of-plane rigid body rotation, and the in-plane rigid body rotation of the projection plane, the pure deformation linear displacement $\Delta\eta_i^d$ and pure deformation angular displacement $\Delta\eta_{\theta i}^d$ of element node i are given by the following equation:

$$\begin{cases} \Delta\boldsymbol{\eta}_a^d = 0, \Delta\boldsymbol{\eta}_i^d = (u_i - u_a) + \Delta\boldsymbol{\eta}_{i-op}^r + \Delta\boldsymbol{\eta}_{i-ip}^r, & (i = b, c, d), \\ \Delta\boldsymbol{\eta}_{\theta i}^d = u_{\theta i} + \Delta\boldsymbol{\eta}_{\theta i-op}^r + \Delta\boldsymbol{\eta}_{\theta i-ip}^r, & (i = a, b, c, d), \end{cases} \qquad (19)$$

2.3. Internal Force of Element Nodes.

When solving the internal forces of element nodes, the VFIFE method transforms the spatial element problem into a planar element problem by defining the deformation coordinate system. The reference element node a is defined as the origin point in this section for the deformation coordinate system, and the $\hat{x}$ axis is defined as the direction along the edge ab of the element, which results in $\hat{u}_a = \hat{v}_a = 0$ and $\hat{w}_i = 0$ $(i = a, b, c, d)$.

The transformational relation between the global coordinate system and the deformation coordinate system is given by the following equation:

$$\hat{\mathbf{x}} = \hat{\mathbf{Q}}(x - x_a), \qquad (20)$$

where $x = \{x \quad y \quad z\}$ is the linear coordinate vector in the deformation coordinate system, $\hat{\mathbf{Q}}$ is the transformation matrix from the global coordinate system to the deformation coordinate system which is given by equation (21). Since $\hat{z} = 0$, $\hat{\mathbf{x}}$ could be simplified to $\hat{\mathbf{x}} = \{\hat{x} \quad \hat{y}\}^T$.

$$\hat{\mathbf{Q}} = \{\hat{\mathbf{e}}_1 \quad \hat{\mathbf{e}}_2 \quad \hat{\mathbf{e}}_3\}^T, \qquad (21)$$

where $\hat{\mathbf{e}}_1 = (\overline{\mathbf{x}}_b - \overline{\mathbf{x}}_a)/|\overline{\mathbf{x}}_b - \overline{\mathbf{x}}_a|, \hat{\mathbf{e}}_3 = \mathbf{n}^0, \hat{\mathbf{e}}_2 = \hat{\mathbf{e}}_3 \times \hat{\mathbf{e}}_1$.

The pure deformation linear displacements vector $\widehat{\mathbf{u}}_i$ and pure deformation angular displacements vector $\widehat{\mathbf{u}}_{\theta i}$ in the deformation coordinate system for the element node i are given by the following equation:

$$\begin{cases} \widehat{\mathbf{u}}_i = \widehat{\mathbf{Q}}\Delta\boldsymbol{\eta}_i^d, & (i = a, b, c, d), \\ \widehat{\mathbf{u}}\theta_i = \widehat{\mathbf{Q}}\Delta\boldsymbol{\eta}_{\theta i}^d, & (i = a, b, c, d), \end{cases} \tag{22}$$

where $\widehat{\mathbf{u}}_i = \left\{ \widehat{u}_i \ \ \widehat{v}_i \ \ \widehat{w}_i \right\}^T$, $\widehat{\mathbf{u}}_{\theta i} = \left\{ \widehat{u}_{\theta i} \ \ \widehat{v}_{\theta i} \ \ \widehat{w}_{\theta i} \right\}$. Since $\widehat{w}_i = 0$ and $\widehat{w}_{\theta i}$ can be not considered in the solving process of the internal forces of element nodes, $\widehat{\mathbf{u}}_i$ and $\widehat{\mathbf{u}}_{\theta i}$ can be simplified as $\widehat{\mathbf{u}}_i = \left\{ \widehat{u}_i \ \ \widehat{v}_i \right\}^T$ and $\widehat{\mathbf{u}}_{\theta i} = \left\{ \widehat{u}_{\theta i} \ \ \widehat{v}_{\theta i} \right\}^T$, respectively.

The pure deformation linear displacements $\widehat{u}_i, \widehat{v}_i$ of element nodes are applied for calculating the node internal forces for membrane element part, the pure deformation linear displacements $\widehat{w}_i$ and pure deformation angular displacements $\widehat{u}_{\theta i}, \widehat{v}_{\theta i}$ of element nodes are applied for calculating the node internal forces and node internal moments for plate element part. Then, the deformation virtual work equation of the quadrilateral shell element is given by the following equation:

$$\sum_i \left\{ \delta\left(\widehat{\mathbf{u}}_{m\_i}\right)^T \widehat{\mathbf{f}}_{m\_i} + \delta\left(\widehat{\mathbf{u}}_{\theta b\_i}'\right)^T \widehat{\mathbf{f}}_{\theta b\_i}' \right\} = \int_V \left\{ \delta\left(\Delta\widehat{\boldsymbol{\varepsilon}}_m\right)^T \widehat{\boldsymbol{\sigma}}_m dV + \delta\left(\Delta\widehat{\boldsymbol{\varepsilon}}_b\right)^T \widehat{\boldsymbol{\sigma}}_b dV \right\}, \tag{23}$$

where $\widehat{\mathbf{u}}_{m\_i} = \left\{ \widehat{u}_i \ \ \widehat{v}_i \right\}^T$ and $\widehat{\mathbf{u}}_{\theta b\_i}' = \left\{ \widehat{w}_i \ \ \widehat{u}_{\theta i} \ \ \widehat{v}_{\theta i} \right\}^T$ are the pure deformation linear displacement vector of node i for membrane element part and the pure deformation linear (angular) displacement vector of node i for plate element part in the deformation coordinate system, respectively.

By introducing the generalized form function of the quadrilateral isoparametric element in traditional finite element, the pure deformation linear displacements vector $\widehat{\mathbf{u}}$ and pure deformation angular displacements vector $\widehat{\mathbf{u}}_\theta$ are shown as equation (24) at any position of elements.

$$\begin{cases} \widehat{\mathbf{u}} = \sum_{i=a,b,c,d} N_i \widehat{\mathbf{u}}_i, \\ \widehat{\mathbf{u}}_\theta = \sum_{i=a,b,c,d} N_i \widehat{\mathbf{u}}_{\theta i}, \end{cases} \tag{24}$$

where $N_i(\widehat{x}, \widehat{y}, \widehat{z})$ is the element form function, whose deformation form is the same as the traditional finite element.

For the quadrilateral isoparametric element with four nodes, the square element coordinates (ξ, η) in the element coordinate system are introduced to solve the relevant variable values in the deformation system, and the expression of the element shape function $N_i(\widehat{x}, \widehat{y}, \widehat{z})$ is shown as the following equation:

$$N_i(\widehat{x}, \widehat{y}, \widehat{z}) = N_i(\xi, \eta) = \frac{1}{4}(1 + \xi_i \xi)(1 + \eta_i \eta), \tag{25}$$

where ξ_i and η_i are the square element coordinates of the four nodes in the element coordinate system, and the value is ± 1.0. The transformation of the element coordinate system and deformation coordinate system is completed in this paper by Jacobian matrix $\mathbf{J}$, whose expression is given in reference [20].

The node pure deformation linear displacement combines the vector of the membrane element part $\widehat{\mathbf{u}}_m^*$ and the node pure deformation linear (angular) displacement combines the vector of the plate element part $\widehat{\mathbf{u}}_b'^*$ in the deformation coordinate system are given by the following equation:

$$\begin{cases} \widehat{\mathbf{u}}_m^* = \left\{ \widehat{\mathbf{u}}_b^T \ \ \widehat{\mathbf{u}}_c^T \ \ \widehat{\mathbf{u}}_d^T \right\}^T, \\ \widehat{\mathbf{u}}_b'^* = \left\{ \widehat{\mathbf{u}}_{\theta a}'^T \ \ \widehat{\mathbf{u}}_{\theta b}'^T \ \ \widehat{\mathbf{u}}_{\theta c}'^T \ \ \widehat{\mathbf{u}}_{\theta d}'^T \right\}^T, \end{cases} \tag{26}$$

where $\widehat{\mathbf{u}}_i = \left\{ \widehat{u}_i \ \ \widehat{v}_i \right\}^T$, $\widehat{\mathbf{u}}_{\theta i}' = \left\{ \widehat{w}_i \ \ \widehat{u}_{\theta i} \ \ \widehat{v}_{\theta i} \right\}^T = \left\{ 0 \ \ \widehat{u}_{\theta i} \ \ \widehat{v}_{\theta i} \right\}^T$.

The tensile strain vector of the membrane element part $\Delta\widehat{\varepsilon}_m$ and bending (including shear) strain vector of the plate element part $\Delta\widehat{\varepsilon}_b$ are given by the following equation:

$$\begin{cases} \Delta\widehat{\boldsymbol{\varepsilon}}_m = \mathbf{B}_m^* \widehat{\mathbf{u}}_m^*, \\ \Delta\widehat{\boldsymbol{\varepsilon}}_b = \mathbf{B}_b'^* \widehat{\mathbf{u}}_b'^* = \begin{bmatrix} \widehat{z}\mathbf{B}_b^* \\ \mathbf{B}_s^* \end{bmatrix} \widehat{\mathbf{u}}_b'^*, \end{cases} \tag{27}$$

where $\Delta\widehat{\boldsymbol{\varepsilon}}_m = \left\{ \Delta\widehat{\varepsilon}_{mx} \ \Delta\widehat{\varepsilon}_{my} \ \Delta\widehat{\gamma}_{mxy} \right\}^T$, $\Delta\widehat{\boldsymbol{\varepsilon}}_b = \left\{ \Delta\widehat{\varepsilon}_{bx} \ \Delta\widehat{\varepsilon}_{by} \ \Delta\widehat{\gamma}_{bxy} \ \Delta\widehat{\gamma}_{byz} \ \Delta\widehat{\gamma}_{bzx} \right\}^T$, $\mathbf{B}_m^*$ and $\mathbf{B}_b'^*$ are the tensile strain-displacement relationship matrix of the membrane element part and bending (including shear) strain-displacement relationship matrix of the plate element part, respectively, $\mathbf{B}_b^*$ and $\mathbf{B}_s^*$ are bending strain-displacement relationship matrix and shear strain-displacement relationship matrix of plate element part. The detailed expressions of $\mathbf{B}_m^*, \mathbf{B}_b'^*, \mathbf{B}_b^*$, and $\mathbf{B}_s^*$ are given in reference [20].

The material stress-strain relationship matrices (i.e., constitutive matrices) of the membrane element part and plate element part are denoted as $\mathbf{D}$ and $\mathbf{D}'$, respectively, which could be linear elastic or elastoplastic. Then, stress vectors for the membrane element part and plate element part are given by the following equation:

$$\begin{cases} \Delta\widehat{\boldsymbol{\sigma}}_m = \mathbf{D}\Delta\widehat{\boldsymbol{\varepsilon}}_m = \mathbf{D}_b \mathbf{B}_m^* \widehat{\mathbf{u}}_m^*, \\ \Delta\widehat{\boldsymbol{\sigma}}_b = \mathbf{D}'\Delta\widehat{\boldsymbol{\varepsilon}}_b = \begin{bmatrix} \mathbf{D}_b & \\ & \mathbf{D}_s \end{bmatrix} \begin{bmatrix} \widehat{z}\mathbf{B}_b^* \\ \mathbf{B}_s^* \end{bmatrix} \widehat{\mathbf{u}}_b'^*, \end{cases} \tag{28}$$

where $\Delta\widehat{\boldsymbol{\sigma}}_m = \left\{ \Delta\widehat{\sigma}_{mx} \ \Delta\widehat{\sigma}_{my} \ \Delta\widehat{\tau}_{mxy} \right\}^T$, $\Delta\widehat{\boldsymbol{\sigma}}_b = \left\{ \Delta\widehat{\sigma}_{bx} \ \Delta\widehat{\sigma}_{by} \ \Delta\widehat{\tau}_{bxy} \ \Delta\widehat{\tau}_{byz} \ \Delta\widehat{\tau}_{bzx} \right\}^T$, $\mathbf{D}_b$ and $\mathbf{D}_s$ are the constitutive matrices of plane strain (including tensile and bending) and shear strain, respectively.

For the case of elastic materials, $\mathbf{D}_b$ and $\mathbf{D}_s$ are given by the following equation:

$$
\left\{
\begin{aligned}
\mathbf{D}_b &= \frac{E}{1 - v^2}
\begin{bmatrix}
1 & v & 0 \\
v & 1 & 0 \\
0 & 0 & \dfrac{(1 - v)}{2}
\end{bmatrix}, \\
\mathbf{D}_s &= kG
\begin{bmatrix}
1 & 0 \\
0 & 1
\end{bmatrix},
\end{aligned}
\right.
\tag{29}
$$

where E is Young modulus, $G = E/[2(1 + v)]$ is shear modulus, v is Poisson's ratio, k is the shear correction coefficient, and $k = 5/6$ is generally taken to consider the shear non-uniform change in the direction of shell thickness.

Considering the influence of transverse shear stress $\widehat{\tau}_{byz}$ and $\widehat{\tau}_{bzx}$ in quadrilateral isoparametric shell element, the right-hand side formula for deformation virtual work equation (23) can be expressed in a more detailed form, which is given by the following equation:

$$
\begin{aligned}
\delta U &= \int_V \delta \left(\Delta \widehat{\boldsymbol{\varepsilon}}_m \right)^T \left(\widehat{\boldsymbol{\sigma}}_{m0} + \Delta \widehat{\boldsymbol{\sigma}}_m \right) dV + \int_V \delta \left(\Delta \widehat{\boldsymbol{\varepsilon}}_b \right)^T \left(\widehat{\boldsymbol{\sigma}}_{b0} + \Delta \widehat{\boldsymbol{\sigma}}_b \right) dV \\
&= \left(\delta \widehat{\mathbf{u}}_m^* \right)^T \left\{ \int_V \left(\mathbf{B}_m^* \right)^T \widehat{\boldsymbol{\sigma}}_{m0} dV + \left(\int_V \left(\mathbf{B}_m^* \right)^T \mathbf{D}_b \mathbf{B}_m^* dV \right) \widehat{\mathbf{u}}_m^* \right\} + \left(\delta \widehat{\mathbf{u}}'^*_b \right)^T \\
&\quad \cdot \left\{ \int_V \begin{bmatrix} \widehat{z} \mathbf{B}_b^* \\ \mathbf{B}_s^* \end{bmatrix}^T \widehat{\boldsymbol{\sigma}}_{b0} dV + \left(\int_V \begin{bmatrix} \widehat{z} \mathbf{B}_b^* \\ \mathbf{B}_s^* \end{bmatrix}^T \begin{bmatrix} \mathbf{D}_b & \\ & \mathbf{D}_s \end{bmatrix} \begin{bmatrix} \widehat{z} \mathbf{B}_b^* \\ \mathbf{B}_s^* \end{bmatrix} dV \right) \widehat{\mathbf{u}}'^*_b \right\},
\end{aligned}
\tag{30}
$$

where $\widehat{\sigma}_{m0}$ and $\widehat{\sigma}_{b0}$ are the initial stresses of the membrane element part and plate element part.

According to the left-hand side formula of the deformation virtual work equation (23), the internal force vector of the membrane element part and plate element part $\widehat{\mathbf{f}}_m^*$ and internal force (moment) vector of plate element part $\widehat{\mathbf{f}}'^*_{\theta b}$ at the end of particle motion time substep can be obtained by the following equation:

$$
\left\{
\begin{aligned}
\widehat{\mathbf{f}}_m^* &= \left\{ \widehat{\mathbf{f}}_{m\_b}^T \quad \widehat{\mathbf{f}}_{m\_c}^T \quad \widehat{\mathbf{f}}_{m\_d}^T \right\}^T = \widehat{\mathbf{f}}_{m0}^* + \Delta \widehat{\mathbf{f}}_m^* = \int_V \left(\mathbf{B}_m^* \right)^T \widehat{\boldsymbol{\sigma}}_{m0} dV + \left\{ \int_{\widehat{A}_a} \left[\int_{-t_a/2}^{t_a/2} \left(\mathbf{B}_m^* \right)^T \mathbf{D}_b \mathbf{B}_m^* d\widehat{z} \right] d\widehat{A}_a \right\} \widehat{\mathbf{u}}_m^*, \\
\widehat{\mathbf{f}}'^*_{\theta b} &= \left\{ \widehat{\mathbf{f}}'^T_{\theta b\_b} \quad \widehat{\mathbf{f}}'^T_{\theta b\_c} \quad \widehat{\mathbf{f}}'^T_{\theta b\_d} \right\}^T = \widehat{\mathbf{f}}'^*_{\theta b0} + \Delta \widehat{\mathbf{f}}'^*_{\theta b} = \int_V \begin{bmatrix} \widehat{z} \mathbf{B}_b^* \\ \mathbf{B}_s^* \end{bmatrix}^T \widehat{\boldsymbol{\sigma}}_{b0} dV + \left\{ \int_{\widehat{A}_a} \int_{-t_a/2}^{t_a/2} \widehat{z}^2 \mathbf{B}_b^* T \mathbf{D}_b \mathbf{B}_b^* d\widehat{z} d\widehat{A}_a + \int_{\widehat{A}_a} \int_{-t_a/2}^{t_a/2} \mathbf{B}_s^* T \mathbf{D}_s \mathbf{B}_s^* d\widehat{z} d\widehat{A}_a \right\} \widehat{\mathbf{u}}'^*_b,
\end{aligned}
\right.
\tag{31}
$$

where $\widehat{\mathbf{f}}_{m\_i} = \left\{ \widehat{f}_{ix} \quad \widehat{f}_{iy} \right\}^T$ is the internal force of node i for membrane element part and plate element part, $\widehat{\mathbf{f}}_{\theta b\_i}' = \left\{ \widehat{f}_{iz} \quad \widehat{f}_{\theta ix} \quad \widehat{f}_{\theta iy} \right\}^T$ is the internal force (moment) of node i for plate element part, t_a is the thickness of ehe shell element, $\widehat{\mathbf{f}}_{m0}^*$ is the internal force vector of the membrane element part and plate element part at the beginning of the particle motion time substep, $\widehat{\mathbf{f}}'^*_{\theta b0}$ is the internal force (moment) vector of plate element part at the beginning of particle motion time substep, $\Delta \widehat{\mathbf{f}}_m^*$ is the internal force increment vector of the membrane element part and plate element part during the particle motion time substep, $\Delta \widehat{\mathbf{f}}'^*_{\theta b}$ is the internal force (moment) increment vector of the plate element part during the particle motion time substep. In addition, the internal force $\widehat{\mathbf{f}}_{m\_a} = \left\{ \widehat{f}_{ax} \quad \widehat{f}_{ay} \right\}^T$ at the reference node a could be obtained from the static equilibrium condition under planar conditions.

The internal forces (moments) for the node i ($i = a$, b, c, d) in the above-given formula are superimposed and extended to obtain the internal force $\widehat{\mathbf{f}}_i = \left\{ \widehat{f}_{ix} \quad \widehat{f}_{iy} \quad \widehat{f}_{iz} \right\}^T$ and internal moment $\widehat{\mathbf{f}}_{\theta i} = \left\{ \widehat{f}_{\theta ix} \quad \widehat{f}_{\theta iy} \quad \widehat{f}_{\theta iz} \right\}^T$ of 3D shell element, where $\widehat{f}_{\theta iz} = 0$. Then, the internal forces (moments) for the node i in the global coordinate system is obtained system through coordinate system transformation from the deformation coordinate. And, the internal force vector $\mathbf{f}_i$ and internal moment $\mathbf{f}_{\theta i}$ for the element node i at the time t are obtained through forward motion transformation, which is given by the following equation:

$$
\left\{
\begin{aligned}
\mathbf{f}_i &= \left[\mathbf{R}_{ip}(\theta_2) \mathbf{R}_{op}(\theta_2) \right] \widehat{\mathbf{Q}}^T \widehat{\mathbf{f}}_i, \\
\mathbf{f}_{\theta i} &= \left[\mathbf{R}_{ip}(\theta_2) \mathbf{R}_{op}(\theta_2) \right] \widehat{\mathbf{Q}}^T \widehat{\mathbf{f}}_{\theta i},
\end{aligned}
\right.
\tag{32}
$$

where $\mathbf{R}_{op}(\theta_2) = [\mathbf{R}_{op}^*(\theta_2) + \mathbf{I}]^T$, $\mathbf{R}_{ip}(\theta_2) = [\mathbf{R}_{ip}^*(\theta_2) + \mathbf{I}]^T$, $\mathbf{R}_{op}^*(\theta_2)$ and $\mathbf{R}_{ip}^*(\theta_2)$ are the out-of-plane and in-plane forward rotational matrices, which are obtained according to

equation (13) and equation (18). The internal force $\mathbf{f}_i$ and internal force (moment) $\mathbf{f}_{\theta i}$ of element node i are applied to particle i in reverse order to obtain the internal force $\mathbf{f}_i^{int}$ and internal force (moment) $\mathbf{f}_{\theta i}^{int}$ transferred from shell element to particle.

It is worth noting that the research topic of this paper is to develop a quadrilateral shell element considering shear deformation under the theoretical framework of the new analysis method VFIFE, rather than to develop a quadrilateral shell element considering shear deformation with better performance based on the traditional finite element method. VFIFE is a new analysis method based on particle motion, which has great advantages in structure discontinuity behavior, dynamic behavior, and other aspects (see Section 1 for details). However, there is no relevant literature on the quadrilateral shell element theory under the VFIFE method. In this paper, considering from the relatively simple quadrilateral shell element (that is, the linear superposition of the quadrilateral isoparametric membrane element and quadrilateral Mindlin plate element), so as to promote and improve the theoretical development and application of VFIFE, and give full play to the advantages of VFIFE method compared with the traditional FE method. Other refined and high-order shell element models considering shear deformation will be further studied in the future.

3. Key Problems and Corresponding Solutions in Numerical Calculation

3.1. Coordinate Definition Modes. The coordinate definition mode I refers to the coordinates of the element nodes when the pure deformation linear (angular) displacement and internal force (moment) of shell element nodes are solved from time t_0 to t, so they need to be on the same reference plane. The four-node shell element is formed into a spatial quadrilateral after undergoing motion and deformation. The projection coordinates ($\overline{\mathbf{x}}_i, \overline{\mathbf{x}}_i{}'$ and $\overline{\theta}_i, \overline{\theta}_i{}'$) for the element

nodes on the reference planes which are perpendicular to the mean normal vector ($\mathbf{n}, \mathbf{n}'$) of the element and passing through the centroid points (C, C') of the original element can be used as the coordinate definition mode I to realize the transformation of the spatial quadrilateral to the planar quadrilateral.

Coordinate definition mode II refers to the coordinates of each particle when the central difference formulas are applied for solving the particle motion equation (1), so it needs to be a unique value. The following two methods can be adopted: (1) the actual coordinates of the particle corresponding to the spatial quadrilateral after the element movement and deformation; (2) I element nodes corresponding to the same single particle in coordinate definition mode I obtained by plane projection do not coincide with each other, so the average coordinate value ($\mathbf{x} = 1/k \sum_{i=1}^{k} \overline{\mathbf{x}}_i$, $\mathbf{x}' = 1/k \sum_{i=1}^{k} \overline{\mathbf{x}}_i{}'$ and $\theta = 1/k \sum_{i=1}^{k} \overline{\theta}_i, \theta' = 1/k \sum_{i=1}^{k} \overline{\theta}_i{}'$) of each element nodes corresponding to the same single particle in coordinate definition mode I can be taken as coordinate definition mode II, where k is the total number for that corresponding element nodes connected to each element by the same single particle.

3.2. Integral of Internal Forces for Element Nodes. When solving the node internal forces and node internal moments for the membrane element part and plate element part of the quadrilateral isoparametric shell element according to equation (31), the numerical integration operation will be involved since the internal stresses and strains of the elements change with their positions. Considering the case of general elastic-plastic material, the integrations along the thickness and element plane are solved by Newton–Cotes integral scheme and 2D Gaussian integral scheme in the traditional finite element method, [21]. The numerical integration formulas of $\Delta\widehat{\mathbf{f}}_m^*$ and $\Delta\widehat{\mathbf{f}}_{\theta b}'^*$ are given by the following equation:

$$
\left\{
\begin{aligned}
\Delta\widehat{\mathbf{f}}_m^* &= \left\{ \int_{\widehat{A}_a} \left[\int_{-t_a/2}^{t_a/2} (\mathbf{B}_m^*)^T \mathbf{D}_b \mathbf{B}_m^* d\widehat{z} \right] d\widehat{A}_a \right\} \widehat{\mathbf{u}}_m^* = \left\{ \int_{-1}^{1}\int_{-1}^{1} \left[\int_{-t_a/2}^{t_a/2} (\mathbf{B}_m^*(\xi,\eta))^T \mathbf{D}_b(\xi,\eta,\widehat{z}) \mathbf{B}_m^*(\xi,\eta) d\widehat{z} \right] |\mathbf{J}(\xi,\eta)| d\xi\, d\eta \right\} \widehat{\mathbf{u}}_m^* \\
&= \left\{ \int_{-1}^{1}\int_{-1}^{1} \left[\sum_{k=1}^{n_1} \mathbf{H}_k \mathbf{F}_{m1}(\xi,\eta,\widehat{z}_k) \right] |\mathbf{J}(\xi,\eta)| d\xi\, d\eta \right\} \widehat{\mathbf{u}}_m^* \cong \left\{ \sum_{i,j=1}^{n_2} H_{ij} \mathbf{F}_{m2}(\xi_i,\eta_j) \right\} \widehat{\mathbf{u}}_m^*, \\
\Delta\widehat{\mathbf{f}}_{\theta b}'^* &= \left\{ \int_{\widehat{A}_a}\int_{-t_a/2}^{t_a/2} \widehat{z}^2 \mathbf{B}_b^* T \mathbf{D}_b \mathbf{B}_b^* d\widehat{z} d\widehat{A}_a + \int_{\widehat{A}_a}\int_{-t_a/2}^{t_a/2} \mathbf{B}_s^* T \mathbf{D}_s \mathbf{B}_s^* d\widehat{z} d\widehat{A}_a \right\} \widehat{\mathbf{u}}_b'^* = \left\{ \int_{-1}^{1}\int_{-1}^{1} \left[\int_{-t_a/2}^{t_a/2} \widehat{z}^2 (\mathbf{B}_b^*(\xi,\eta))^T \mathbf{D}_b(\xi,\eta,\widehat{z}) \mathbf{B}_b^*(\xi,\eta) d\widehat{z} \right] |\mathbf{J}(\xi,\eta)| d\xi\, d\eta \right. \\
&\quad + \left. \int_{-1}^{1}\int_{-1}^{1} \left[\int_{-t_a/2}^{t_a/2} (\mathbf{B}_s^*(\xi,\eta))^T \mathbf{D}_s(\xi,\eta,\widehat{z}) \mathbf{B}_s^*(\xi,\eta) d\widehat{z} \right] |\mathbf{J}(\xi,\eta)| d\xi\, d\eta \right\} \widehat{\mathbf{u}}_b'^* \\
&= \left\{ \int_{-1}^{1}\int_{-1}^{1} \left[\sum_{k}^{n_1} H_k \widehat{z}_k^2 \mathbf{F}_{b1}(\xi,\eta,\widehat{z}_k) \right] |\mathbf{J}(\xi,\eta)| d\xi\, d\eta + \int_{-1}^{1}\int_{-1}^{1} \left[\sum_{k}^{n_1} \mathbf{H}_k \mathbf{F}_{s1}(\xi,\eta,\widehat{z}_k) \right] |\mathbf{J}(\xi,\eta)| d\xi\, d\eta \right\} \widehat{\mathbf{u}}_b'^* \cong \left\{ \sum_{i,j=1}^{n_2} H_{ij} \mathbf{F}_{b2}(\xi_i,\eta_j) + \sum_{i,j=1}^{n_2} H_{ij} \mathbf{F}_{s2}(\xi_i,\eta_j) \right\} \widehat{\mathbf{u}}_b'^*,
\end{aligned}
\right.
$$

$$(33)$$

where $\mathbf{F}_{m1}(\xi, \eta, \hat{z})$, $\mathbf{F}_{m2}(\xi, \eta)$, $\mathbf{F}_{b1}(\xi, \eta, \hat{z})$, $\mathbf{F}_{b2}(\xi, \eta)$, $\mathbf{F}_{s1}(\xi, \eta, \hat{z})$, and $\mathbf{F}_{s2}(\xi, \eta)$ are given by equation (34), $|\mathbf{J}(\xi, \eta)|$ is the Jacobian determinant, n_1 is the total integral points along the direction of element thickness, and n_2 is the total integral points along the direction of each natural coordinate axis (i.e., square element coordinate axis) in the element reference plane.

$$\begin{cases} \mathbf{F}_{m1}(\xi, \eta, \hat{z}) = \left(\mathbf{B}_m^*(\xi, \eta)\right)^T \mathbf{D}_b(\xi, \eta, \hat{z}) \mathbf{B}_m^*(\xi, \eta), \\ \mathbf{F}_{m2}(\xi, \eta) = \left[\sum_{k=1}^{n_1} \mathbf{H}_k \mathbf{F}_{m1}(\xi, \eta, \hat{z}_k)\right] |\mathbf{J}(\xi, \eta)|, \\ \mathbf{F}_{b1}(\xi, \eta, \hat{z}) = \left(\mathbf{B}_b^*(\xi, \eta)\right)^T \mathbf{D}_b(\xi, \eta, \hat{z}) \mathbf{B}_b^*(\xi, \eta), \\ \mathbf{F}_{b2}(\xi, \eta) = \left[\sum_{k=1}^{n_1} \mathbf{H}_k \hat{z}_k^2 \mathbf{F}_{b1}(\xi, \eta, \hat{z}_k)\right] |\mathbf{J}(\xi, \eta)|, \\ \mathbf{F}_{s1}(\xi, \eta, \hat{z}) = \left(\mathbf{B}_s^*(\xi, \eta)\right)^T \mathbf{D}_s(\xi, \eta, \hat{z}) \mathbf{B}_s^*(\xi, \eta), \\ \mathbf{F}_{s2}(\xi, \eta) = \left[\sum_{k=1}^{n_1} \mathbf{H}_k \mathbf{F}_{s1}(\xi, \eta, \hat{z}_k)\right] |\mathbf{J}(\xi, \eta)|. \end{cases} \quad (34)$$

4. Realization of Nonlinear Material Constitutive

The bilinear elastoplastic constitutive model is widely used in nonlinear analysis of structures considering the linear plastic hardening effect, which is used in this paper for theoretical derivation and numerical analysis.

4.1. Bilinear Elastoplastic Constitutive Model.
Considering the case of isotropic material constitution, the dynamic yield stress is obtained by scaling static yield stress through plastic factor, and its constitutive equation is given by the following equation:

$$\sigma_d = \left(\sigma_0 + E_p \bar{\varepsilon}_p\right), \quad (35)$$

where E_p is the plastic hardening modulus, $E_p = (E_t E)/(E - E_t)$, E is the Young modulus, E_t is the tangent modulus, σ_0 is the static yield stress, $\bar{\varepsilon}_p = \sqrt{(2\varepsilon_{ij,p}\varepsilon_{ij,p})/3}$ is the equivalent plastic strain, $\varepsilon_{ij,p}$ is the plastic strain tensor.

This constitutive model is suitable for bilinear elastic-plastic materials. The case of $E_t = 0$ corresponds to the ideal elastic-plastic model, and the case of $\sigma_0 \gg \sigma$ corresponds to the linear elastic model.

The von Mises yield criterion is adopted in this paper as a dynamic yield criterion, that is, the plastic stress state (i.e., yield condition equation) is given by the following equation:

$$\phi = \bar{\sigma} - \sigma_d = 0, \quad (36)$$

where $\bar{\sigma}$ is the equivalent von Mises stress, which is given by equation (37), σ_d is the dynamic yield stress.

$$\bar{\sigma} = \sqrt{\frac{3}{2} s_{ij} s_{ij}} = \sqrt{\frac{3}{2} \left(\sigma_{ij} - \delta_{ij}\sigma_m\right)\left(\sigma_{ij} - \delta_{ij}\sigma_m\right)}, \quad (37)$$

where $\sigma_m = (\sigma_{11} + \sigma_{22} + \sigma_{33})/3$ is the mean principal stress, σ_{ij} is the stress component, s_{ij} is the deviatoric stress component, $\delta_{ij} = 1 (i \neq j)$, $\delta_{ij} = 0 (i = j)$.

For shell element, the principal stress along the thickness direction of element σ_{33} is always zero, that is $\sigma_{33} = 0$. Accordingly, the transverse principal strain along the thickness direction of element ε_{33} is an dependent variable, which is given by the following equation:

$$\varepsilon_{33} = -\frac{v}{1 - v}\left(\varepsilon_{11} + \varepsilon_{22}\right). \quad (38)$$

In process of solving the elastic-plastic incremental matrix constitutive $\mathbf{D}_{ep}$, the 6×6 elastic constitutive matrix $\mathbf{D}_e$ containing all stress-strain components is used for theoretical derivation. The elastic stress-strain relationship used for trial calculation is given by the following equation:

$$\Delta \hat{\boldsymbol{\sigma}} = \mathbf{D}_e \Delta \hat{\boldsymbol{\varepsilon}}, \quad (39)$$

where $\mathbf{D}_e$ is given by equation (40), $\Delta\hat{\sigma} = \left\{ \Delta\hat{\sigma}_{11} \ \Delta\hat{\sigma}_{22} \ \Delta\hat{\sigma}_{33} \ \Delta\hat{\tau}_{12} \ \Delta\hat{\tau}_{23} \ \Delta\hat{\tau}_{31} \right\}^T$ is the stress increment vector, $\Delta\hat{\varepsilon} = \left\{ \Delta\hat{\varepsilon}_{11} \ \Delta\hat{\varepsilon}_{22} \ \Delta\hat{\varepsilon}_{33} \ \Delta\hat{\gamma}_{12} \Delta\hat{\gamma}_{23} \Delta\hat{\gamma}_{31} \right\}^T$ is the strain increment vector.

$$\mathbf{D} = \frac{E}{1 - v^2} \begin{bmatrix} 1 & v & 0 & 0 & 0 & 0 \\ v & 1 & 0 & 0 & 0 & 0 \\ \dfrac{(1-v)v}{1-2v} & \dfrac{(1-v)v}{1-2v} & \dfrac{(1-v)^2}{1-2v} & 0 & 0 & 0 \\ 0 & 0 & 0 & \dfrac{1-v}{2} & 0 & 0 \\ 0 & 0 & 0 & 0 & k\dfrac{1-v}{2} & 0 \\ 0 & 0 & 0 & 0 & 0 & k\dfrac{1-v}{2} \end{bmatrix}, \quad (40)$$

where E is Young modulus, k is the shear correction coefficient, and v is Poisson's ratio, which are given in equation (29).

4.2. Plastic Incremental Analysis Steps.
Given the initial stress and strain at the beginning of the time substep and the incremental strain during the time substep, the elastic-plastic incremental analysis is used to obtain the updated stresses and strains under the condition for satisfying the material constitutive and yield criteria at the end of time substeps. Detailed steps are as follows:

> Step 1: elastic prediction. The stress component $\sigma_{ij,t}$ and the equivalent plastic strain $\bar{\varepsilon}_{p,t}$ at the time t (i.e., at the beginning of time substep) and the incremental strain component $\Delta\hat{\varepsilon}_{ij}$ from the time t to the time $t + \Delta t$ (i.e., during the time substep) are given. Assuming that the time substep is completely elastic, the predicted elastic

stress matrix $\sigma_{tr,t+\Delta t}$ and the predicted plastic hardening parameter matrix $\kappa_{tr,t+\Delta t} = E_{p,t+\Delta t}\overline{\varepsilon}_p$ at the time $t + \Delta t$ are obtained.

Step 2: yield judgment. Substitute $\sigma_{tr,t+\Delta t}$ and $\kappa_{tr,t+\Delta t}$ at the time $t + \Delta t$ into the yield condition equation (36), and judge whether it is an elastic or plastic incremental time substep according to the positive or negative of the predicted yield function $\phi_{tr,t+\Delta t}$. If $\phi_{tr,t+\Delta t} > 0$, it is a plastic time substep; Otherwise, it is an elastic time substep.

Step 3: plastic correction. If it is an elastic incremental time substep, then skip this step. If it is a plastic incremental time substep, the plastic flow factor increment $\Delta\lambda$ is calculated on the basis of normal flow rule and dynamic yield criterion. The case of $\Delta\lambda > 0$ corresponds to the plastic incremental time substep, and the case of $\Delta\lambda = 0$ corresponds to the elastic incremental time substep.

Step 4: stress and strain updating. If it is an elastic incremental time substep, then $\sigma_{t+\Delta t} = \sigma_{tr,t+\Delta t}$. If it is a plastic incremental time substep, the stress and strain updating is carried out by $\Delta\lambda$. The updated variables include the equivalent plastic strain $\overline{\varepsilon}_{p,t+\Delta t}$, the dynamic yield stress $\sigma_{d,t+\Delta t}$, the deviatoric stress component $s_{ij,t+\Delta t}$, the von Mises stress $\overline{\sigma}_{t+\Delta t}$ and the actual stress $\sigma_{t+\Delta t}$ at the time $t + \Delta t$.

Step 5: solution of the elastic-plastic matrix. If it is an elastic time substep, there is no plastic matrix $\mathbf{D}_p$. If it is a plastic time substep, the elastic-plastic matrix $\mathbf{D}_{ep}$ needs to be solved. Through dynamic yield criterion and normal flow rule, the plastic flow factor increment $d\lambda$ and plastic matrix $\mathbf{D}_p$ are obtained, and then $\mathbf{D}_{ep} = \mathbf{D}_e - \mathbf{D}_p$. Then, the internal forces (moments) of element nodes are solved by integral formulas.

5. Programming and Example Verification

Based on the above-given theoretical formulas of vector quadrilateral isoparametric shell element with shear deformation, a computational analysis program is developed by Matlab software to realize the calculation and analysis of shell structure with shear deformation. The program implementation process is shown in Figure 1. Then, the rationality and practicability of derived formulas and program codes are verified by the following examples.

5.1. Static Bending of Annular Thick-Plate (Shear Effect along Thickness). Taking an annular thick-plate with circular line load as an example [22], the influence of the shear effect along thickness for shell element on small bending deformation of thick plate structure is studied. Figure 2 shows the typical annular thick-plate structure, including the geometric model and mesh model. The inner radius of plate is $R_1 = 1.4$ in, the outer radius of the plate is $R_2 = 2.0$ in and the thickness of plate is $t_a = 0.5$ in (corresponding width-thickness ratio is $(R_2 - R_1)/t_a = 1.2 < 5$, that is, thick plate). The plate is placed horizontally and initially at rest. The

boundary conditions for the inner circular edge and outer circular edge are respectively simply supported and free. The line loading $q = 800$ lb/in is loaded on the circular line at the radius $R = 1.8$ in of the annular thick-plate, and the static results are obtained by applying damping to eliminate the dynamic oscillation effect. The mass density is $\rho = 0.1$ lbs/in^3, the Young modulus is $E = 1.8 \times 10^7$ lb/in^2 and the 'Poisson's ratio is $v = 0.3$. The quadrilateral isoparametric shell element is used for numerical simulation. The time substep is $h = 6.0 \times 10^{-6}$ s and the damping parameter $\alpha = 2 \times 10^4$.

In order to investigate the influence of different mesh sizes on the VFIFE method in this paper, the mesh sizes l are set as 0.05 in, 0.10 in, and 0.20 in, respectively, for solving calculation. Figure 3 shows the comparison of vertical displacement convergence values of the outer-edge nodes with different mesh sizes. It can be seen that with the decrease of element mesh size, the vertical displacement decreases and the decreasing speed becomes slow. Therefore, the element mesh size l of 0.10 in is selected for in-depth analysis in the following, which has a relatively small calculation scale and high calculation accuracy.

In order to investigate the influence of different thicknesses on the VFIFE method in this paper, the shell thicknesses t_a are set as 0.1~1.5 in (the corresponding length-to-thickness L/t_a is 6~0.4), respectively, for solving calculation. Figure 4 shows the comparison of vertical displacement convergence values of the outer-edge nodes with different shell thicknesses. It can be seen that when $t_a \geq 0.5$ in (that is $t_a/l \geq 5$, which belongs to medium-thick shell, corresponding to $L/t_a = 1.2$), the error between the VFIFE method and ANSYS calculation results is relatively small, and the calculation accuracy of the VFIFE method in this paper is improved with the increase of shell thickness. When $t_a < 0.5$ (that is, belonging to thin-shell), the error between the VFIFE method and ANSYS calculation results is relatively large. When $t_a \leq 0.2$, the thick-shell element superimposed by the VFIFE method is not applicable, so there is no corresponding calculated value. Therefore, for the medium-thick shell element with $t_a/l \geq 5$, the VFIFE method has a high accuracy.

Figure 5 shows the computational convergence process for the vertical displacements of outer-edge nodes of the annular thick-plate with the mesh size l of 0.10 in. The result shows that it has good convergence and the vertical displacement convergence result is about 0.00533 in. Figure 6 shows the calculated results of the vertical displacements and von Mises stresses for radial nodes along the radial direction (corresponding to radial distance) of the annular thick-plate, respectively, and the comparison with ANSYS calculated results including that with shear effect (i.e., ANSYS-shear) and without shear effect (i.e., ANSYS-no-shear). Among them, I results of the cases for ANSYS-shear and ANSYS-non-shear are obtained by applying the shell43 element (considering Mindlin–Ressner first-order shear effect) and shell63 element (considering no shear effect), respectively.

The result from Figure 6 shows that the vertical displacements of the outer circular edge node of the annular thick-plate calculated by the method of this paper (i.e., VFIFE), ANSYS-shear, and ANSYS-no-shear are 0.00533 in,
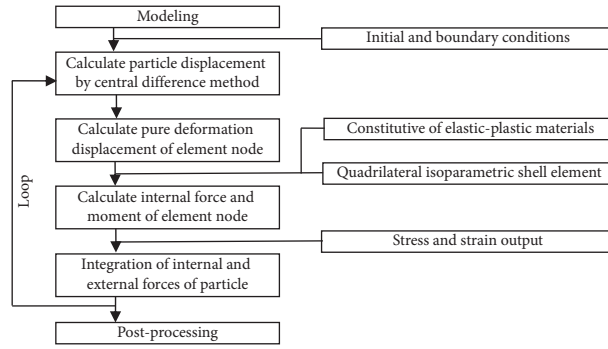
Figure 1: Analysis flow chart for shell structures.

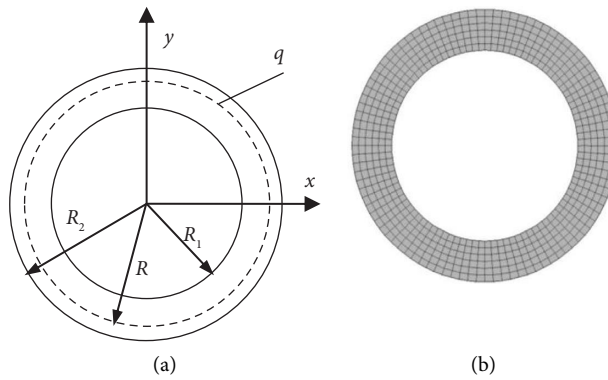(a)   (b)

Figure 2: Annular thick-plate model. (a) Geometric model. (b) Mesh model.
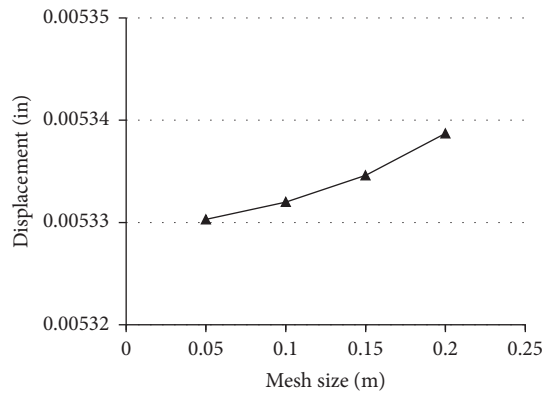

Figure 3: Comparison of vertical displacements of outer-edge nodes with different mesh sizes ($t_a = 0.5$ in).

0.00534 in and 0.00521 in respectively. The errors of the displacement results of VFIFE are about 0.18% compared with the results of ANSYS-shear and about 2.31% compared with the results of ANSYS-no-shear considering the influence of shear deformation. The calculated result is basically consistent with the result in literature [22]. The case of results for von Mises stress is similar, that is, the maximum errors of the von Mises stress results of VFIFE are about 0.37% compared with the results of ANSYS-shear and about 2.58% compared with the results of ANSYS-no-shear. The calculated results of the proposed method in this paper (i.e., VFIFE method) are close to those of ANSYS-shear, which

verifies the correctness and effectiveness of the VFIFE method. For the thick-plate structure, the shear effect has a certain influence, and the VFIFE method presented here has good accuracy for analyzing the thick-plate structure with shear deformation. With the increase of plate thickness, the shear effect cannot be ignored gradually.

The quadrilateral shell element of the VFIFE method in this paper is based on the linear superposition of the quadrilateral isoparametric membrane element and quadrilateral Mindlin isoparametric plate element, which is mainly applied for medium-thick shell structures. For thin shell structures, in addition to the low calculation accuracy,
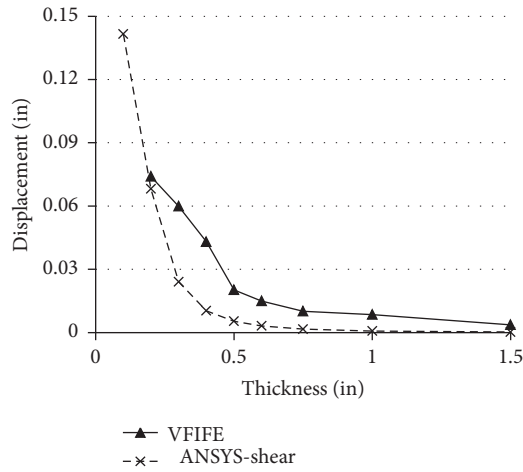
FIGURE 4: Comparison of vertical displacements of outer-edge nodes with different thicknesses (mesh size is 0.10 in).
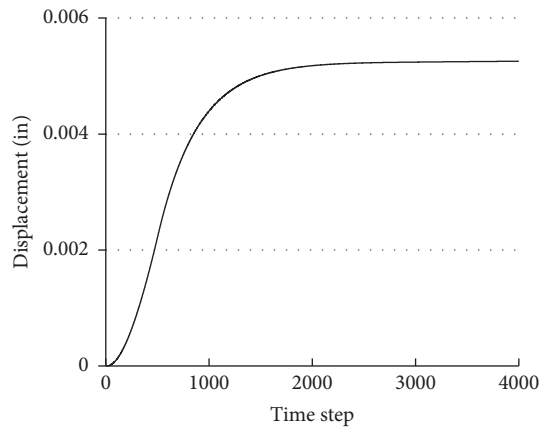

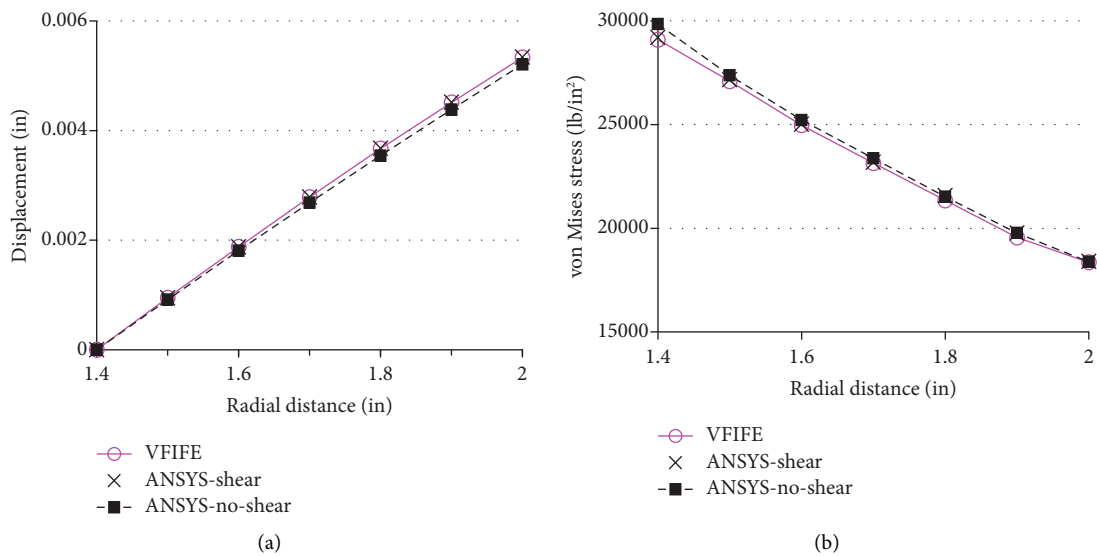FIGURE 5: Convergence process of vertical displacement for outer-edge node.

FIGURE 6: Results of the radial nodes along the radial direction. (a) Vertical displacement. (b) Von mises stress (SNEG surface).

there is also a shear self-locking phenomenon. Due to the complexity of this problem, this paper did not make a detailed analysis and considered further research.

5.2. Dynamic Bending of Long Cantilever Plate (Large Displacement and Rotation).

Taking a long cantilevered plate with a concentrated load at its cantilevered end as an example [23]. Figure 7 shows the typical cantilevered plate structure, including the geometric model and mesh model. The width of the plate is $B = 0.2$ m, the length of plate is $L = 1.0$ m and the thickness of plate is $t_a = 0.015$ m. The plate is placed horizontally and initial at rest. The boundary conditions for one end and other end are, respectively, fixed and free cantilever. The concentrated load $P = 100$ kN is loaded on the midpoint of the cantilevered end for the plate. The ramp-platform dynamic loading mode is adopted, and the convergence value is achieved through damping. The mass density is $\rho = 7850$ kg/m^3, the Young modulus is $E = 201$ GPa and the 'Poisson's ratio is $v = 0.3$. The quadrilateral isoparametric shell element is used for numerical simulation. The time substep is $h = 2.0 \times 10^{-6}$ s and the damping parameter $\alpha = 200$.

The four cases of quadrilateral shell element (i.e., the superposition of quadrilateral membrane elements and Mindlin plate elements) in this paper with shear correction coefficients $k = 5/6, 2/3, 1/3, 0$ and the case of triangular shell element in literature [23] (i.e., the superposition of CST membrane element and DKT plate element) without shear deformation are considered for analysis and comparison. Figure 8 shows the vertical displacement-time curves for a long cantilevered plate at the central node of the free end, which shows good convergence under quasi-static calculation.

It can be observed from Figure 8 that the vertical displacement convergence values of the free end central node for the long cantilevered plate calculated by the VFIFE method of this paper with shear correction coefficients $k = 5/6, 2/3, 1/3,$ and 0 are about 0.186 m, 0.227 m, 0.369 m, and 0.983 m, respectively, and that of literature [23] without shear deformation is 0.800 m. The vertical displacement at the central node for free end with $k = 5/6$ (i.e., general shear) is only about 19% and 23% of that with $k = 0$ (i.e., no shear) and that of literature [23], respectively. For long cantilever shell structures, the shear effect of shell element is extremely significant and cannot be ignored. In this case, the triangular shell element without shear deformation given in literature [23] is no longer applicable, and the quadrilateral isoparametric shell element with shear deformation given in this paper should be adopted.

In addition, the vertical displacement-time variation curves of the quadrilateral shell element with $k = 0$ (i.e., no shear) and the nonshear triangle shell element given in reference [23] are basically consistent before the time of 0.02 s, which also verifies the practicability of the proposed method (VFIFE) in a certain extent.

Figure 9 shows the displacement deformation diagrams of the long cantilever plate with shear correction coefficients $k = 5/6, 2/3, 1/3,$ and 0 at the time of 0.04 s. It can be observed

from Figure 9 that the long cantilever plate with a shear deformation effect presents a bending-shear bending form, which is a process of large displacement and large rotation. Taking the case of $k = 5/6$ as an example, Figure 10 shows the von Mises stress contours (MATLAB self-programming is used to draw) of the long cantilever plate at the time of 0.04 s. It turned out from Figure 10 that maximum stress appears in the root region of the long cantilever plate.

In the above, Figure 9 is not a curve, but a side view of the long cantilever plate with large displacement and rotation, which reflects the applicability of the VFIFE method in this paper under the condition of large deformation and rotation. As for the quantitative analysis of deformation under different shear coefficients, it has been described in Figure 8 and above.

5.3. Nonlinear Stability Analysis of Shallow Spherical Shell (Elastic-Plastic Material Constitutive).

Taking a jump instability of the shallow spherical shell with the central concentrated load as an example [24], the influence of elastic-plastic material constitutive for shell element on nonlinear stability is studied. Figure 11 shows the typical shallow spherical shell structure, including the geometric model and mesh model. The spherical radius of shell is $R = 2.54$ m, the projected side length of shell is $L = 1.5698$ m and the thickness of shell is $t_a = 99.45$ m. The shell is placed horizontally and initial at rest. The boundary conditions are that four sides are simply supported. The concentrated load P is loaded on the central node of shell. The mass density is $\rho = 2500$ kg/m^3, the Young modulus is $E = 68.95$ MPa and the Poisson's ratio is $v = 0.3$. The quadrilateral isoparametric shell element is used for numerical simulation. The time substep is $h = 2.0 \times 10^{-4}$ s and the damping parameter $\alpha = 20$. The whole process of elastic-plastic instability of the shallow spherical shell is tracked by the displacement control method.

Figure 12 shows the concentrated load-vertical displacement curves for the central node of the shallow spherical shell. It can be observed that with the increases of the vertical displacement for the central nodes, there is an obvious load extreme point of the shallow spherical shell. After crossing the extreme point, the vertical displacement deformation turns over greatly and the load drops sharply. At this time, the structure cannot be used normally due to the excessive deformation, that is, the jump buckling occurs. After complete overturning, the load continues to increase with the increase of structural vertical displacement.

There are some differences in the load-displacement process between the VFIFE method of this paper and the ABAQUS method, but the overall changing trend is consistent, and the load extreme points are about the same. The maximum extreme point loading from the VFIFE method is about 16.45 kN when the vertical displacement is about 210 mm, and that from the ABAQUS method is about 18.76 kN, with an error of about 12.3%, which is relatively small. The calculation errors mainly come from the error of solving the jump instability problem and the number of shell elements. The error can be further reduced with the increase
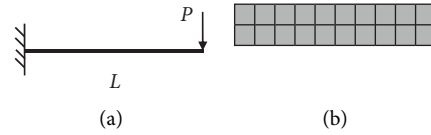
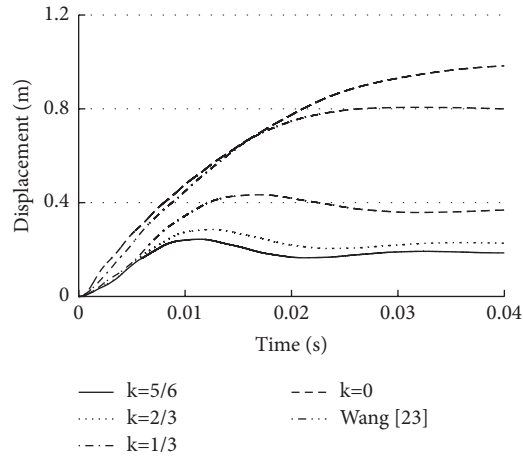FIGURE 7: Long cantilevered plate model. (a) Geometric model. (b) Mesh model.

FIGURE 8: Vertical displacements-time curves at the central node of the free end.
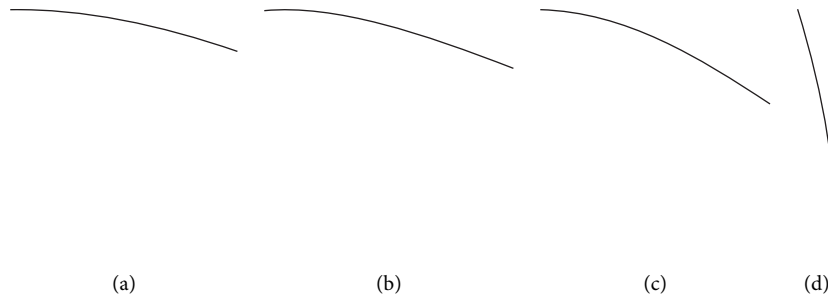

FIGURE 9: Displacement deformation diagrams. (a) $k = 5/6$ (b) $k = 2/3$ (c) $k = 1/3$ (d) $k = 0$.
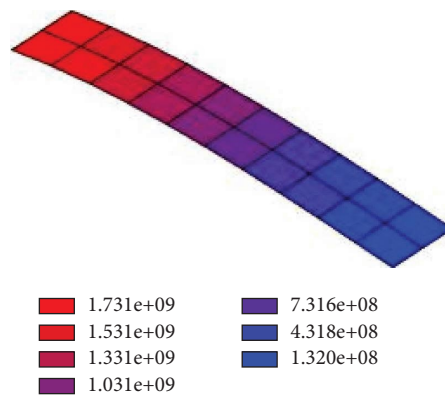

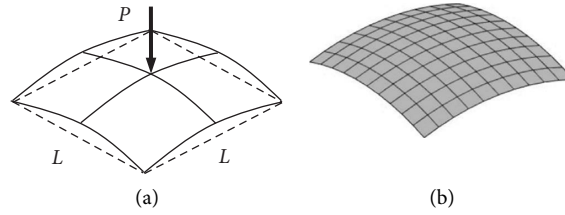FIGURE 10: Von mises stress contours of the long cantilevered plate at the time of 0.04 s.

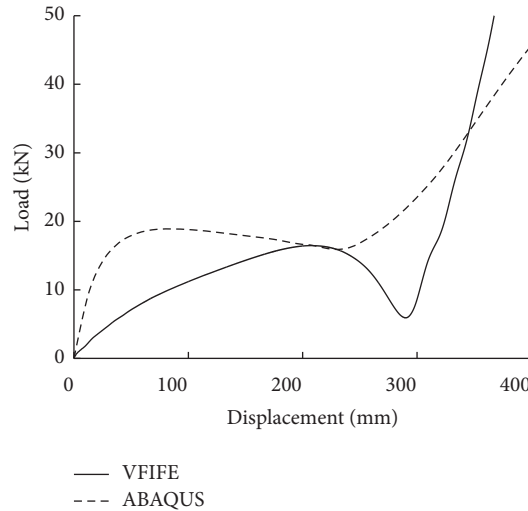FIGURE 11: Shallow spherical shell model. (a) Geometric model. (b) Mesh model.

FIGURE 12: Load-displacement curves for center nodes of the shallow spherical shells.

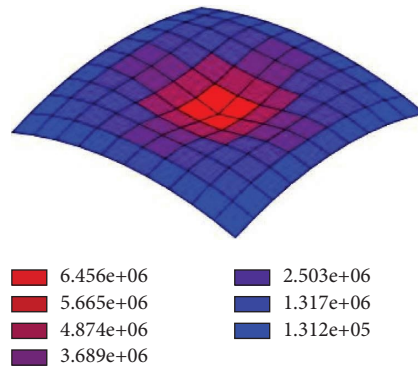|	
6.456e+06	2.503e+06
5.665e+06	1.317e+06
4.874e+06	1.312e+05
3.689e+06	

FIGURE 13: Von mises stress contours of the shallow spherical shell.

of the number of shell elements. As for the large difference between VFIFE and ABAQUS results in Figure 12, it may be related to the loading path and displacement accumulation effect of the buckling problem involving large deformation and abrupt deformation. However, the buckling extreme points are basically the same, which verifies the effectiveness of this method to some extent.

Figure 13 shows the von Mises stress contours (MAT-LAB self-programming is used to draw) of the shallow spherical shell when the maximum extreme point load (corresponding to the vertical displacement 210 mm) is reached by the VFIFE method. It can be observed from

Figure 13 that the region near the central node is in a state of plastic hardening due to the concentrated load.

6. Conclusions

In this paper, the theory and application for the quadrilateral isoparametric shell elements based on the VFIFE method are researched, and the following conclusions are obtained:

(1) Based on the linear superposition of the quadrilateral isoparametric membrane elements and the quadrilateral Mindlin plate elements, the basic vector

formula of the quadrilateral isoparametric shell element with shear deformation is derived. Two different coordinate modes for updating the particle displacement and the element node internal force are proposed. The uniform solution of the irregular quadrilateral element is realized by the isoparametric integral scheme along the element plane.

(2) The bilinear elastoplastic constitutive model for the material is introduced into vector finite shell elements, and the nonlinear effect of the material is realized based on the integral method along the thickness of the element.

(3) Based on the established basic theory of quadrilateral isoparametric shell elements with vector finite element, the corresponding calculation, and analysis program is developed. Example analysis shows that the vector finite element program can obtain good computational accuracy in the static and dynamic analysis, large deformation, and large rotation analysis for shell structure, which verifies the rationality and practicability for derived formulas and program codes.

(4) VFIFE method is applied to the stability analysis for shell structures with double nonlinearity including geometric nonlinearity and material nonlinearity. By means of displacement control, the jump instability process of plate and shell structure can be obtained without special treatment, and the critical loading can be obtained, which reflects the advantages of this method in analyzing the stability problems of material with large deformation and rotation and elastic-plastic.

Data Availability

The data used to support the findings of this study are included within the article.

Conflicts of Interest

The authors declare that they have no conflicts of interest.

Acknowledgments

References

[1] D. Dinh-Cong and T. Nguyen-Thoi, "A new efficient two-stage method for damage localization and quantification in shell structures," *Applied Soft Computing*, vol. 108, Article ID 107468, 2021.

[2] Q. Zhang, S. F. Li, A. M. Zhang, and Y. Peng, "On nonlocal geometrically exact shell theory and modeling fracture in shell structures," *Computer Methods in Applied Mechanics and Engineering*, vol. 386, Article ID 114074, 2021.

[3] A. Hajlaoui, E. Chebbi, and F. Dammak, "Three-dimensional thermal buckling analysis of functionally graded material structures using a modified FSDT-based solid-shell element," *International Journal of Pressure Vessels and Piping*, vol. 194, Article ID 104547, 2021.

[4] Z. Soltani and S. A. Hosseini Kordkheili, "Interlaminar stress analysis of composite shell structures using a geometrically nonlinear layer-wise shell finite element," *Composite Structures*, vol. 257, Article ID 113074, 2021.

[5] A. Muc, M. Chwał, and M. Barski, "Remarks on experimental and theoretical investigations of buckling loads for laminated plated and shell structures," *Composite Structures*, vol. 203, pp. 861–874, 2018.

[6] B. E. Green, D. R. Strome, and R. C. Weikel, "Application of the stiffness method to the analysis of shell structures," in *Proceedings of the Procedures on Aviation Conference*, American Society of Mechanical Engineers (ASME), Los Angeles, LA, USA, March, 1961.

[7] O. C. Zienkiewicz, *The Finite Element Method in Engineering Science*, McGraw-Hill, New York, NY, USA, 2nd ed edition, 1971.

[8] K. J. Bathe and L. W. Ho, "A simple and effective element for analysis of general shell structures," *Computers & Structures*, vol. 13, no. 5-6, pp. 673–681, 1981.

[9] H. T. Y. Yang, S. Saigal, A. Masud, and R. K. Kapania, "A survey of recent shell finite elements," *International Journal for Numerical Methods in Engineering*, vol. 47, no. 1-3, pp. 101–127, 2000.

[10] Q. S. Wang, D. Shao, and B. Qin, "A simple first-order shear deformation shell theory for vibration analysis of composite laminated open cylindrical shells with general boundary conditions," *Composite Structures*, vol. 184, pp. 211–232, 2018.

[11] M. Lezgy-Nazargah and S. Salahshuran, "A new mixed-field theory for bending and vibration analysis of multi-layered composite plate," *Archives of Civil and Mechanical Engineering*, vol. 18, no. 3, pp. 818–832, 2018.

[12] M. Lezgy-Nazargah, "A high-performance parametrized mixed finite element model for bending and vibration analyses of thick plates," *Acta Mechanica*, vol. 227, no. 12, pp. 3429–3450, 2016.

[13] M. Lezgy-Nazargah and Z. Meshkani, "An efficient partial mixed finite element model for static and free vibration analyses of FGM plates rested on two-parameter elastic foundations," *Structural Engineering & Mechanics*, vol. 66, no. 5, pp. 665–676, 2018.

[14] E. C. Ting, C. Shih, and Y. K. Wang, "Fundamentals of a vector form intrinsic finite element: Part I. Basic procedure and a plane frame element," *Journal of Mechanics*, vol. 20, no. 2, pp. 113–122, 2004.

[15] E. C. Ting, C. Shih, and Y. K. Wang, "Fundamentals of a vector form intrinsic finite element: Part II. Plane solid elements," *Journal of Mechanics*, vol. 20, no. 2, pp. 123–132, 2004.

[16] C. Shih, Y. K. Wang, and E. C. Ting, "Fundamentals of a vector form intrinsic finite element: Part III. Convected material frame and examples," *Journal of Mechanics*, vol. 20, no. 2, pp. 133–143, 2004.

[17] T. Y. Wu, C. Y. Wang, C. C. Chuang, and E. C. Ting, "Motion analysis of 3D membrane structures by a vector form intrinsic finite element," *Journal of the Chinese Institute of Engineers*, vol. 30, no. 6, pp. 961–976, 2007.

[18] Z. Wang, K. Hu, and Y. Zhao, "Triangular thin-shell element of Vector Form Intrinsic Finite Element considering Cowper-

Symonds viscoplastic material constitutive model," *Journal of Building Structures*, vol. 35, no. 4, pp. 71–77, 2014.

[19] Z. Wang, Y. Zhao, and K. Hu, "Triangular thin-plane element based on vector form intrinsic finite element," *Engineering Mechanics*, vol. 31, no. 1, pp. 37–45, 2014.

[20] R. Q. Xu, *Finite Element Method Structural Analysis and MATLAB Programming*, pp. 178–181, China Communication Press, Beijing, China, 2006.

[21] X. C. Wang, *Finite Element Method*, pp. 145–149, Tsinghua University Press, Beijing, China, 2008.

[22] R. J. Roark and W. C. Young, *Formulas for Stress and Strain*, pp. 376–380, McGraw-Hill Book Company, Inc, New York, NY, USA, 5nd ed edition, 1975.

[23] Z. Wang, Y. Zhao, and K. Hu, "Triangular thin-shell element based on vector form intrinsic finite element," *Journal of Building Structures*, vol. 35, no. 4, pp. 64–70, 2014.

[24] G. Horrigmoe and P. G. Bergan, "Nonlinear analysis of free-form shells by flat finite elements," *Computer Methods in Applied Mechanics and Engineering*, vol. 16, no. 1, pp. 11–35, 1978.